Pressure transducer for measuring acoustic radiation force based on a magnetic sensor

H A S Kamimura[1]**, T Z Pavan**[1]**, T W J Almeida**[1]**, M L A Pádua**[1]**,
A L Baggio**[1]**, M Fatemi**[2] **and A A O Carneiro**[1]

[1] Departamento de Física e Matemática, Faculdade de Filosofia, Ciências e Letras de Ribeirão Preto,
Universidade de São Paulo, Ribeirão Preto, São Paulo, Brazil
[2] Department of Physiology and Biomedical Engineering, College of Medicine, Mayo Clinic, Rochester,
Minnesota, USA

E-mail: adilton@usp.br

Abstract

This work presents a pressure transducer based on a magnetic sensor to measure acoustic
radiation force (ARF) and small displacements. The methodology presented in this paper
allowed this transducer to be calibrated for use as an acoustic pressure and intensity meter. It
can control the acoustic intensity emitted by ultrasound used, for example, in ARF impulse
imaging, vibro-acoustography and high-intensity focused ultrasound techniques. The device
comprises a magnet, a membrane, a magnetoresistive sensor and a coil to cancel the external
magnetic field. When ARF is applied to the membrane, the magnetic field on the sensor
changes due to the magnetic target displacement. The variation of the output signal from the
magnetic transducer is proportional to the acoustic pressure applied to the membrane. A
focused ultrasound transducer with a central frequency of 3 MHz was used to apply a
continuous ARF. The sensitivities of the magnetic transducer as an acoustic pressure and
intensity meter, evaluated in water, were respectively 0.597 μV MPa^{-1} and
0.073 μV (W cm^{-2})$^{-1/2}$, while those of the needle hydrophone (Onda model HNP-0400) used
in the magnetic transducer calibration were respectively, 0.5024 mV MPa^{-1} and
6.153 mV (W cm^{-2})$^{-1/2}$. The transducer resolution to displacement is 5 nm and 6 dB of
signal attenuation occurs for 7° of misalignment. The transducer responded well to acoustic
pressure in water above 200 kPa.

Keywords: acoustic pressure, acoustic radiation force, magnetic sensor, ultrasound

1. Introduction

The acoustic power emitted by ultrasound transducers used
for medical purposes must be controlled. Quantification of
ultrasound power is the main parameter for assessing safety
of transducers. To ensure the quality of these techniques, a
methodology or a device for monitoring the acoustic output
may be used.

The acoustic power can be estimated through acoustic
radiation force (ARF) detection. The sound waves exert force
(static or dynamic) on an object by transferring part of their
momentum. The static force is generated by a continuous-
wave ultrasound beam. In the dynamic case, the ultrasound
radiation force is generated by an amplitude-modulated (AM)
wave. The dynamic radiation force can be generated by the
interference of two continuous-wave ultrasound beams. A
detailed description of the theory of ARF in fluids was given
by Silva *et al* [1].

The acoustic output of medical ultrasonic equipment is
characterized via either an ARF balance, which determines
the total output power, or a piezoelectric hydrophone, which
determines the spatial and temporal distribution of the acoustic
pressure [2].

Radiation force balances employ targets made of different absorbing materials and electronic balances for measuring the time-averaged force exerted by the acoustic field reaching the absorbing target. A power balance system based on a conical float suspended in water, which intercepts the acoustic field, was presented by Wong *et al* [3]. Power balances available have sensitivity levels in the range of 200 mW to 12 W, typically used in physiotherapy [2].

Typical acoustic pressure in medical diagnostic systems is 4 MPa for peak compressional pressure [4]. Hydrophones based on membranes manufactured from a piezoelectric polymer—polyvinylidene fluoride (pvdf)—are considered to be the gold standard for acoustic pressure measurement. The sensitive part of hydrophones, which defines the spatial resolution of the device, is commonly of sub-mm diameter. Typical membranes have a spatial resolution in the range of 0.3 to 0.5 mm and frequency resonance in the range of 30 to 50 MHz. Needle hydrophones have a spatial resolution in the range of 0.04 to 0.12 mm and a complex frequency response above 1 MHz [2].

In the last two decades, ARF has become an important tool in therapeutic applications and for analyzing the viscoelastic properties of biological tissues. Some examples of these techniques are as follows.

- *ARF impulse imaging* [5] *and supersonic imaging* [6]: a pulsed focused ultrasound beam (spatial peak temporal average intensity approaching 1000 W cm^{-2}) causes tissue displacement in a small region of interest. Time and spatial information of transverse wave propagation allows us to analyze the mechanical properties of the material under study [7]. It is possible to generate mechanical property images of organs such as the liver [8], arteries [9] and others [10, 11].

- *Vibro-acoustography*: two cofocused ultrasound beams with slightly different frequencies cause a low frequency movement in the focal region [12]. The acoustic intensity range used in vibro-acoustography for human diagnostic applications is under 720 mW cm^{-2}, but Chen *et al* [13] showed that intensities up to 200 W cm^{-2} are still safe for analyzing soft tissue. This vibration emits a sound that is detected by a low-frequency hydrophone. The amplitude and phase of this vibration depend on the viscoelastic properties of the target and the surrounding tissue. Typical modulated frequencies in vibro-acoustography are lower than 100 kHz [14]. Differences in vibro-acoustographic response may indicate changes in viscoelastic and other properties of tissue, which may represent an abnormality of the tissue [15].

- *High-intensity focused ultrasound (HIFU)*: a high-power focused ultrasound beam (with intensities up to 2000 W cm^{-2}) is applied to a small volume of tissue, increasing the local temperature with low dissipation on adjacent tissues [16]. This feature allows for the ablation of tumors, preventing injuries to healthy tissues [17].

- *Ultrasound physiotherapy*: a low-intensity ultrasound (0.125–3 W cm^{-2}) interacts with tissue and the energy of the wave is attenuated. The energy deposition by absorption causes tissue heating and nonthermal effects
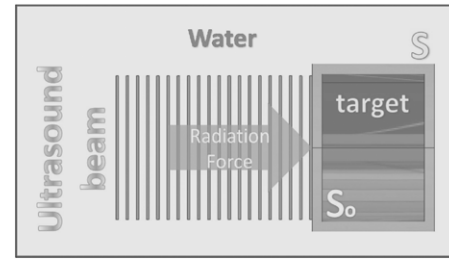

Figure 1. The radiation force due to an ultrasound beam hitting a magnetic target. The acoustic radiation is attenuated by the target, causing a force and moving it.

to it [18], e.g., it stimulates tissue repairing and wound healing [19] or accelerates healing in bone fractures [20].

Carneiro *et al* [21] previously showed computational simulations for an idealized experimental setup using magnetic measurement techniques for monitoring ARF. They simulated the variations of the magnetic field emitted by a magnetic target embedded in a soft medium in response to the radiation force of an AM ultrasound beam. In this work, we explore the potential of that methodology in the construction of a balance transducer for monitoring the ARF generated by an ultrasound transducer.

A methodology to quantify the acoustic radiation of ultrasound transducers was developed. The developed prototype measures the displacement of a magnet by detecting the variation of its magnetic field on a magnetic sensor. The displacement indicates the acoustic pressure and the acoustic intensity emitted by the ultrasound transducer. The device works as a high-sensitivity pressure transducer and could also be used as a device for nano-displacement measurements.

2. Materials and methods

2.1. Radiation force analysis

An ultrasound beam traveling in a lossless liquid medium of density ρ reaching a totally absorbing target will cause an instantaneous net force $\vec{f}$ displacing this target. This displacement is related to the amplitude of the force, morphology of the target, viscoelasticity and density of the target and the medium surrounding it [22]. Figure 1 shows an illustrative picture of an ultrasound force applied on a target immersed in water. The target surface (S_0) has the same dimension as the cross-sectional area of the ultrasound beam.

The phenomenon of radiation force depends on the interaction of second-order acoustic fields with the target [1]:

$$\vec{f} = -\rho_0 \frac{\mathrm{d}}{\mathrm{d}t} \left(\int_S \phi^{(1)} \vec{n} \, \mathrm{d}S + \int_{S_0} \phi^{(2)} \vec{n} \, \mathrm{d}S \right) - \int_{S_0} \vec{n} . \vec{T} \, \mathrm{d}S \quad (1)$$

where $\phi^{(1)}$ and $\phi^{(2)}$ are the linear and second-order velocity potentials, respectively, and $\vec{n}$ is the outward normal unit-vector of the integration surface. The quantity $\vec{T}$ is the radiation-stress tensor.
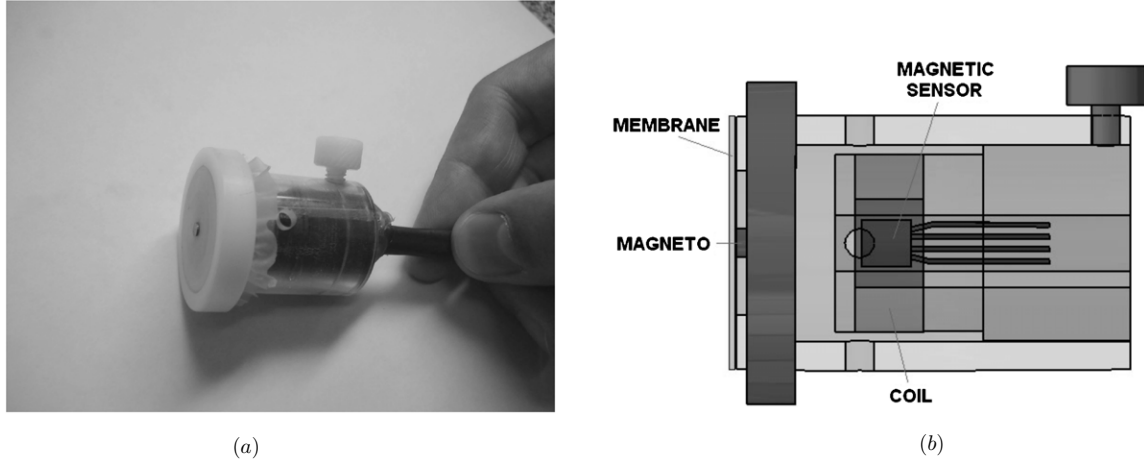
Figure 2. Magnetic transducer: (*a*) photograph and (*b*) schematic.

Table 1. Characteristics of magnetic sensor KMZ10A[a].

Parameter	Value
Dimensions (length × width × thickness)	$17.7 \times 4.4 \times 1.6$ mm³
Sensitivity	$16 \frac{\text{mV/V}}{\text{kA/m}}$
Temperature coefficient of bridge resistance (-25 to $+125\,°$C)	0.25% K^{-1}
Operating frequency	0 to 1 MHz

[a] Data extracted from manufacturer's datasheet.

To analyze the frequency spectrum of the net force acting on the object, we take the Fourier transform of equation (1) as follows:

$$\hat{\vec{f}}(\omega) = -j\omega\rho_0 \mathcal{F}\left[\int_S \phi^{(1)} \vec{n} \, dS\right] - j\omega\rho_0 \int_{S_0} \mathcal{F}[\phi^{(2)}] \vec{n} \, dS - \int_{S_0} \vec{n}.\mathcal{F}[\vec{T}] \, dS. \tag{2}$$

Given that the device presented in this paper is composed of a magnet fixed to a membrane, which does not have resonance components in high frequencies, it vibrates for low-frequency applied radiation forces and displaces statically for high-frequency applied radiation forces. Since the radiation force applied to the target studied in this work, as can be seen in section 2.3.2, is high frequency, it is considered to be a static radiation force problem, and the static component ($\omega = 0$) of (2) gives

$$\vec{f}_S = -\int_{S_0} \vec{n}.\mathcal{F}[\vec{T}]_{\omega=0} \, dS. \tag{3}$$

For a long time interval the time average of $\vec{T}$ is $\langle\vec{T}\rangle = \mathcal{F}[\vec{T}]_{\omega=0}$, so

$$\vec{f}_S = -\int_{S_0} \vec{n}.\langle\vec{T}\rangle \, dS. \tag{4}$$

The static radiation force generated by attenuation of the ultrasound beam by the target is given by equation (4).

2.2. The magnetic transducer

A magnetic sensor, Philips model KMZ10A, which employs the magnetoresistive effect of thin film permalloy materials to measure weak pressures, was adopted. Its characteristics are presented in table 1. This sensor employs four magnetoresistive elements placed as a Wheatstone bridge where an externally applied magnetic field promotes a variation to the generated signal by the sensor [23]. An offset coil was placed surrounding the magnetic transducer to compensate the DC external magnetic fields, which could influence the measurements. In front of the magnetic sensor (1 cm away) was placed a cylindrical NdFeB magnet (diameter = 2.9 mm and length = 2 mm) fixed on a latex membrane, keeping the axial symmetry of the magnet coinciding with the maximum sensitive direction of the magnetic sensor. The absolute magnetic field, 1 cm away from the surface of the magneto, is about 5 μT. A prototype of this transducer is shown in figure 2. When a force is applied to the sensor, the membrane is deformed, moving the magnet and changing the magnetic field reaching the sensor. On the sides of the transducer, holes were made for air or water to flow freely to avoid restraining membrane movement.

The sensitivity of this pressure transducer was evaluated in and out of water.

2.3. Transducer calibration

2.3.1. Out of water. The sensitivity and linearity of the system, as a force and position transducer, were characterized using a micrometer (0.005 mm resolution) and a digital scale (0.01 g resolution). This procedure allows for a direct relation of the sensor output signal with the applied pressure and membrane displacement. Since the sensor is sensitive to the variation of the magnetic field in two directions, the setup was built to guarantee that the membrane displacement occurred only toward the sensors (figure 3).

When a micrometer displacement (D) was applied to the magnetic target, a force (F) was simultaneously registered through the scale. The displacement and pressure calibration
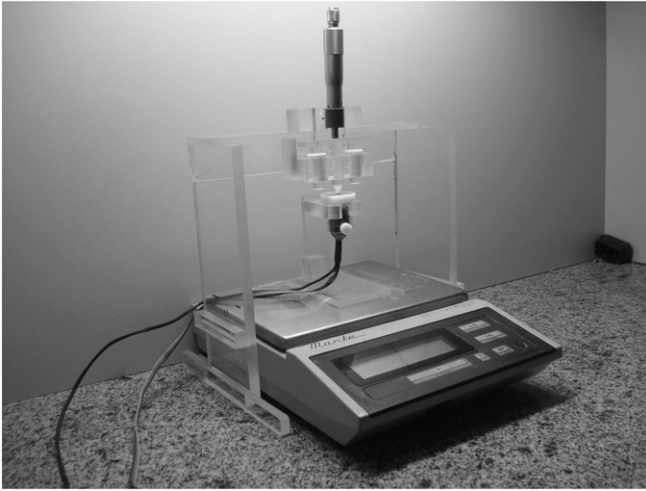
Figure 3. Experimental setup to calibrate the magnetic transducer using a digital scale.

Figure 4. Experimental setup to measure the acoustic radiation force of an ultrasound transducer.

factors C_{Da} and C_{Pa} were obtained following equations (5) and (6):

$$V = C_{Da} D \tag{5}$$

$$V = C_{Pa} P \tag{6}$$

where V is the output signal of the magnetic sensor in volts and P is the pressure on the target generated by the mechanical force. The pressure on the magnetic target was estimated by

$$P = \frac{F}{A} \tag{7}$$

where $A = \pi \cdot r^2$ (magnet area = 6.605 mm^2)

The transducer output signals were evaluated as a function of pressure and the magnet displacement generated by a tight and static force. This force was evaluated through a digital scale placed on the bottom of the transducer.

2.3.2. In water. The potential of the magnetic transducer for measuring ARF was evaluated using a focused ultrasound transducer composed of a spherical piezoelectric element of 43 mm diameter, 7 cm focus depth and a central frequency of 3 MHz. The maximum temporal average intensity of the ultrasound beam was evaluated through a needle hydrophone (Onda model HNP-0400) placed in the focus region. The calibration factors provided by Onda Corporation for a frequency of 3 MHz are 5.024×10^{-8} V Pa^{-1} and 3.786×10^{-5} V^2 cm^2 W^{-1}. This procedure was done to relate the magnetic transducer response to the acoustic power and acoustic pressure in the focus region.

The resolution of the magnetic transducer as a displacement transducer was evaluated using a laser vibrometer (Polytec model PDV-100). It was performed by modulating the ARF by an AM wave and measuring the vibration amplitude of the target using the laser vibrometer and the magnetic transducer simultaneously.

The magnetic transducer was placed in front of the ultrasound transducer in its focus region (figure 4). The piezoelectric ele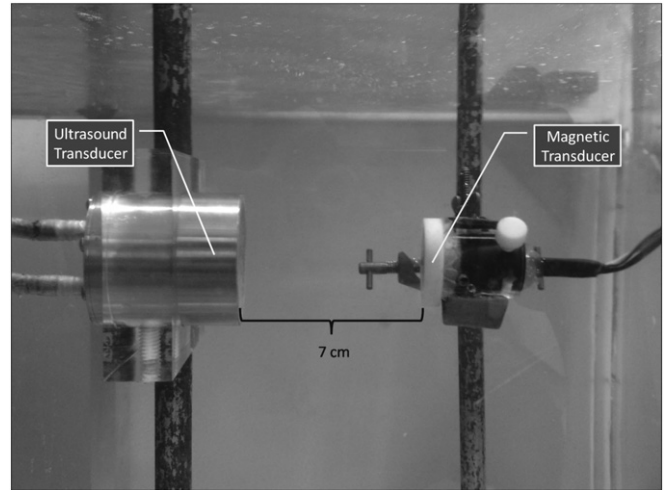ment was driven with a continuous sinusoidal wave using a signal generator (Tektronix model AFG320) and a homemade power amplifier of 20 dB. The range of voltage applied to the ultrasound transducer was 8.25 V to 49.5 V due to power amplifier limitation (maximum output voltage of 50 V).

The angular response of the magnetic transducer was evaluated by moving the ultrasound transducer around the magnetic transducer using a stepper motor (1.8° resolution). The focus of the ultrasound radiation field was kept in the center of the target during the procedure. The voltage applied to the ultrasound transducer was 33 V and the angular range evaluated was −54° to +54°.

3. Results

Figure 5 shows the output of the magnetic transducer as a function of (*a*) pressure applied to the magnetic target, and (*b*) its displacement evaluated in air environment. The sensitivities of the magnetic transducer as a pressure and displacement sensor, considering a unitary gain, were $C_{Pa} = 5.09$ mV kPa^{-1} and $C_{Da} = 44.3$ mV mm^{-1}. These factors were obtained from the angular coefficients of the linear fitting of the curves in figure 5.

The maximum pressure and the temporal average intensity of the ultrasound beam measured at the focus of the transducer as a function of voltage applied on the piezoelectric ceramic are shown in figure 6.

According to the plot in figure 6, the calibration curves for pressure and intensity are given by

$$P_w = 5.16 \times 10^{-2} \times V \tag{8}$$

$$I = 17.6 \times 10^{-2} \times V^2 \tag{9}$$

where P_w is the acoustic pressure (MPa), I is the acoustic intensity (W cm^{-2}) and V is the ultrasound-applied voltage (V). Equations (8) and (9) relate acoustic pressure and intensity to the voltage applied to the ultrasound transducer. The following calibration curves used these relations to determine the acoustic pressure and intensity applied to the magnetic
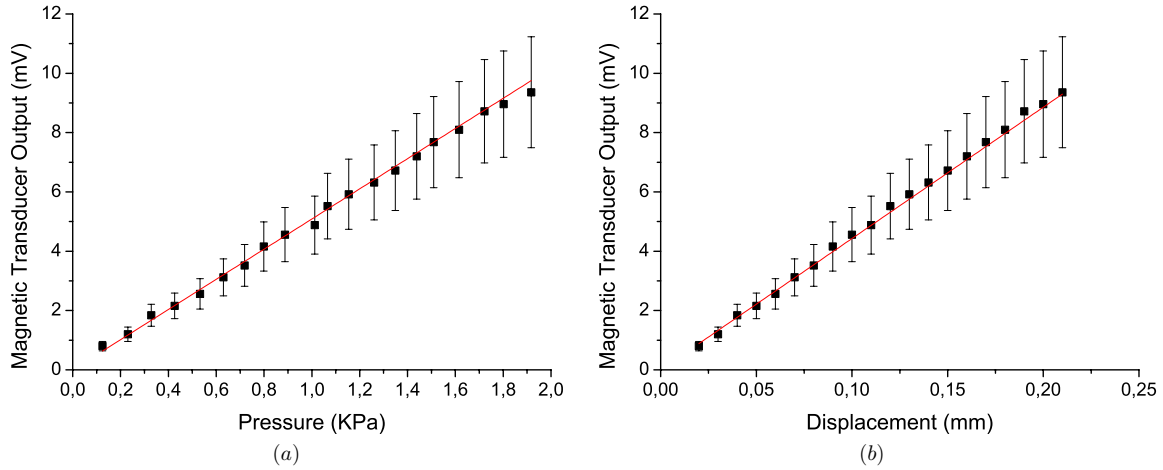
Figure 5. Calibration curves of the magnetic transducer, in air environment, as a function of (*a*) pressure and (*b*) displacement.
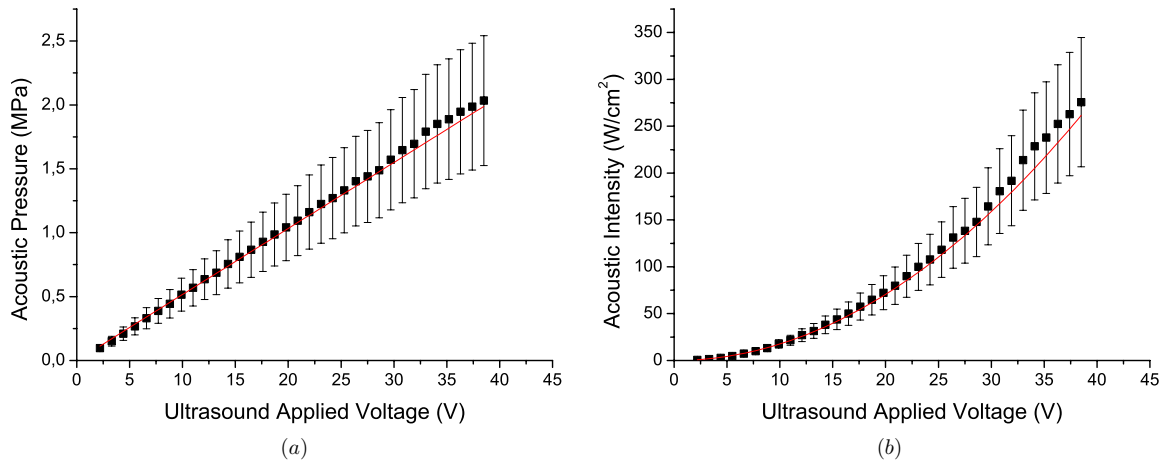

Figure 6. Calibration of the ultrasound transducer using a needle hydrophone. (*a*) Acoustic pressure and (*b*) acoustic intensity.

transducer. Figure 7 shows the response of the magnetic transducer to a range of voltage applied to the ultrasound transducer in a 2 second acquisition window. In this case, the acoustic force on the target began after 1 second of acquisition.

Figure 8 shows the calibrated curves of the magnetic transducer for ultrasound pressure and average ultrasound intensity. They were estimated from the minimum value, after the impulse peak (1 s of acquisition), presented in the high-level output voltage shown in figure 7.

According to figure 8, the response of the magnetic transducer was linear with the acoustic pressure. The calibration relations from the curves of this transducer for pressure and intensity from ultrasound radiation force immersed in water are given by

$$S = 0.597 \times P \qquad (10)$$
$$S = 0.073 \times I^{0.5} \qquad (11)$$

where S is the magnetic transducer signal (μV), P is the acoustic pressure (MPa) and I is the acoustic intensity (W cm^{-2}).

The magnetoresistive sensor used has a magnetic field resolution of the order of 5 nT, and works for a range of
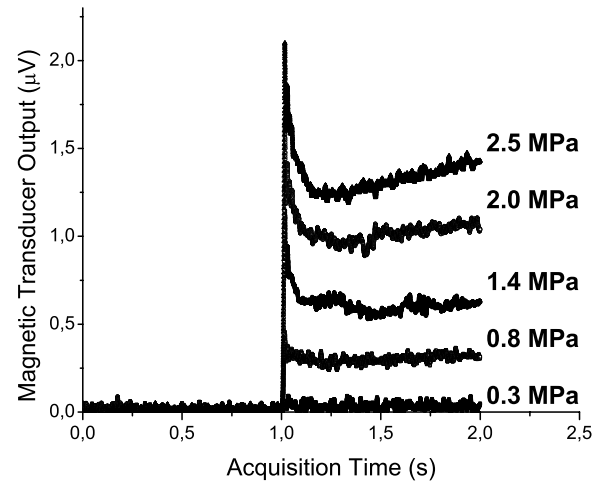

Figure 7. Profile of the magnetic transducer output versus time. The beginning of the acoustic force on the target was after 1 second of acquisition.

± 5 mT. Its resolution as a displacement measure of the magnetic target position is about 5 nm. As a pressure transducer, the device was more sensitive for the measurement
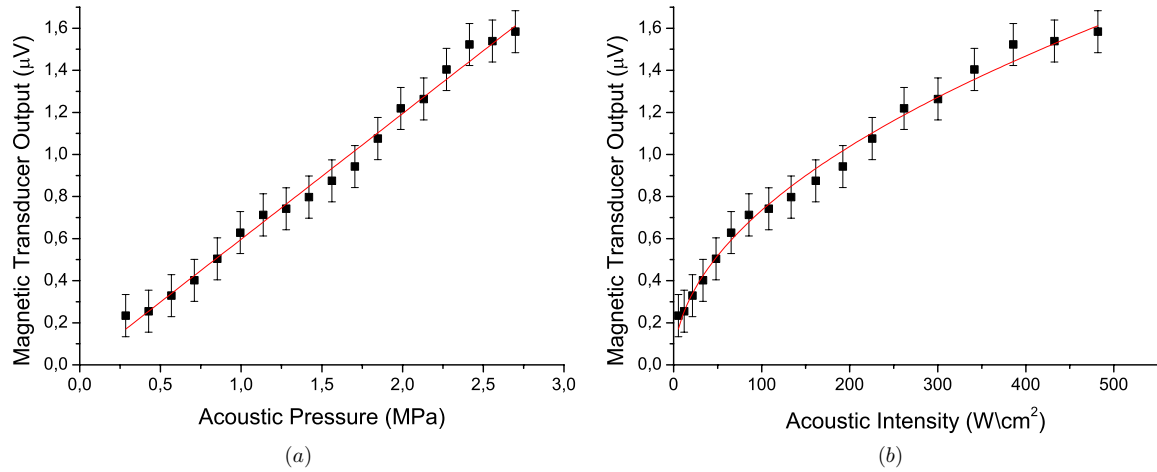
Figure 8. Response of the magnetic transducer as a function of (*a*) pressure and (*b*) intensity due to the ultrasound radiation force generated by the focused transducer.
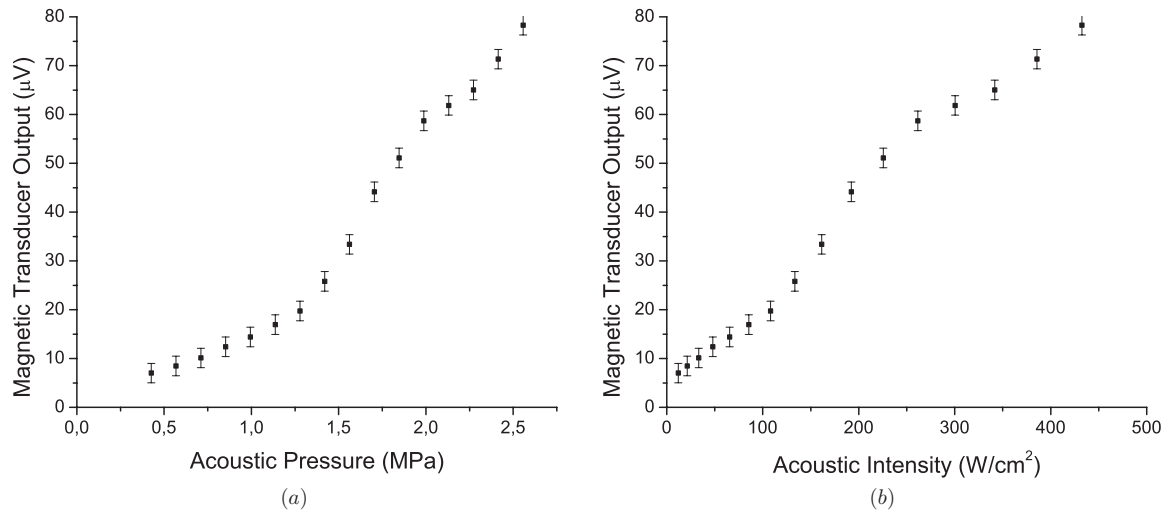

Figure 9. Calibration curves of the magnetic transducer as a function of (*a*) acoustic pressure and (*b*) acoustic intensity, obtained from the measurement of the stabilized output signal.

in air than in water. The range of the evaluated pressures using this prototype was [0.1 kPa–2 kPa] in air and [0.2 MPa–3 MPa] in water.

As shown in figure 7, the response of the transducer peaked immediately after the transducer response, then increased slowly until becoming stable. Figure 9 shows the nonlinear behavior for the signal output measured after the membrane stabilization. The stabilization times of the output signal were expanded, increasing the ultrasound beam energy. Using this procedure of measurements, the response profile of the magnetic transducer can be considered linear just for low acoustic pressures (under 1.3 MPa). Figure 10 shows the angular sensitivity of the magnetic transducer. The −6 dB attenuation occurred for 7° of misalignment. For angles smaller than 4°, the response variation is about 10%.
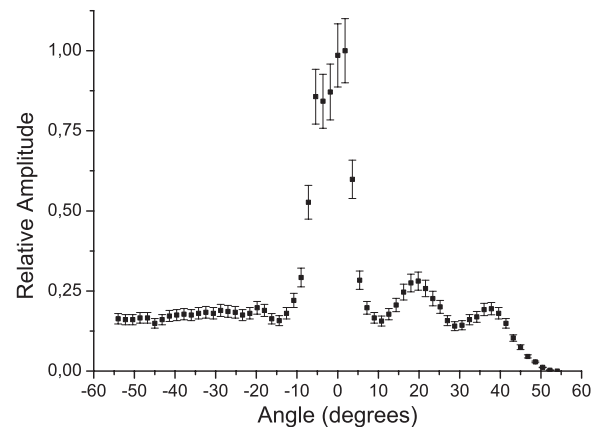
4. Discussion

The methodology presented in this paper showed a new instrument based on a magnetic sensor to evaluate the pressure

Figure 10. Angular sensitivity of the magnetic transducer.

generated by ultrasound radiation force as well as to estimate micrometer displacement simultaneously due to the action of this force on a membrane. The device works for both static

and modulated force. For example, when applying a constant amplitude ultrasound field, the displacement on the magnetic target will be static and the variation of the magnetic field on the magnetic sensor is linearly proportional to the ultrasound radiation pressure.

The measurements in air showed that the transducer response was linear with the displacement. Regarding the measurement of pressures, no comparison can be made with the measurements in air and in water since the resistance and viscoelasticity of the medium (membrane and water) significantly changed the membrane movement and the stabilization time of the transducer response. Comparing the responses in figure 8 and figure 9, we can see that the transducer output magnitude was around 50 times higher for measurements taken after the membrane stabilization than the 1 s acquisition measurements.

As observed in figure 6, the pressure from focused ARF used to evaluate the magnetic transducer was linear. According to figure 8, the profile response of the magnetic transducer was linear with the acoustic radiation pressure when its output signal was read in the minimal amplitude condition. But, it was not linear if the output signal was read after its stabilization (see figure 9). This nonlinearity behavior is attributed to the morphology of the transducer and viscoelasticity of the medium (membrane and water). For measurements performed in air, this nonlinearity was not observed and the digital scale stabilized instantly. However, in water, the viscosity changed its flow out of the transducer, causing a damping on the membrane movement. A factor contributing to the water flux resistance while the membrane is being pushed could be the size of the hole (see figure 2). For measurements in water, stabilization times were needed (several minutes) between measurements. After the discontinuity of the radiation force, a relaxation time of the membrane was also necessary to perform a new measurement.

As shown in figure 9, the membrane displacement after stabilization of the system can be considered linear for pressures lower than 1.3 MPa. On the other hand, for applied pressures higher than 1.3 MPa, a short tone burst pulse can be used to minimize this slow displacement of the membrane. Thus, this magnetic transducer is more feasible to evaluate the power of pulsed ultrasound radiation force. However, the magnetic transducer can also be applied to continuous wave, as long as the output signal is measured in a short time (<2 s). The dependence of the output signal on the mechanical resistance of the medium (water + membrane) suggests a feasibility study of this transducer as a viscoelasticity meter.

For misalignments smaller than $4°$, the variation on output signal is less than 10%. The sensitivities of the magnetic transducer obtained for unitary gains were 0.597 μV MPa^{-1} and 0.073 μV (W cm^{-2})$^{-1/2}$, as an acoustic pressure and intensity meter.

Even though the transducer was characterized as a balance to evaluate ultrasound radiation force, it can be used for other applications to evaluate small pressures and displacement. For the prototype presented in this work, we were able to evaluate the acoustic pressures in water as low as 0.2 MPa. These limitations are due to the stiffness of the membrane.

Membranes with different stiffnesses could be employed depending on the application. Membranes with a higher elastic modulus could be used to measure higher pressures, as is found in HIFU, for instance. Membranes with a lower elastic modulus could be an alternative to measure lower pressures.

5. Conclusion

The magnetic transducer presented here can be used as an ultrasound power balance to measure both continuous waves and pulsed waves. The results found suggest that this transducer could be a powerful tool to evaluate the ultrasound radiation force generated by techniques such as ARF impulse, HIFU and vibro-acoustography. The ARF measurement using a transducer based on the magnetic sensor can be a suitable method for evaluating the spatial power distribution of high-intensity ultrasound beams. The results showed that the magnetic transducer produced results comparable to results obtained with a needle hydrophone for measuring acoustic intensity and sound pressure. Therefore, the magnetic transducer presented here may be used as a low-cost and robust instrument for calibrating and characterizing ultrasound transducers.

Acknowledgments

References

[1] Silva G T, Chen S, Greenleaf J F and Fatemi M 2005 Dynamic ultrasound radiation force in fluids *Phys. Rev.* E **71** 056617

[2] Zeqiri B 2007 Metrology for ultrasonic applications *Prog. Biophys. Mol. Biol.* **93** 138–52

[3] Wong G S K and Wu L 2002 High power ultrasound standard *J. Acoust. Soc. Am.* **111** 1791

[4] Duck F A and Martin K 1993 Exposure values for medical devices *Ultrasonic Exposimetry* ed M C Ziskin and P A Lewin (Boca Raton, FL: CRC Press) pp 315–44

[5] Nightingale K, Soo M S, Nightingale R and Trahey G 2002 Acoustic radiation force impulse imaging: in vivo demonstration of clinical feasibility *Ultrasound Med. Biol.* **28** 227–35

[6] Bercoff J, Tanter M and Fink M 2004 Supersonic shear imaging: a new technique for soft tissue elasticity mapping *IEEE Trans. Ultrason. Ferroelectr. Freq. Control* **51** 396–409

[7] Dumont D, Dahl J, Miller E, Allen J, Fahey B and Trahey G 2009 Lower-limb vascular imaging with acoustic radiation force elastography: demonstration of in vivo feasibility *IEEE Trans. Ultrason. Ferroelectr. Freq. Control* **56** 931–44

[8] Fahey B J, Hsu S J, Wolf P D, Nelson R C and Trahey G E 2006 Liver ablation guidance with acoustic radiation force impulse imaging: challenges and opportunities *Phys. Med. Biol.* **51** 3785

[9] Trahey G E, Palmeri M L, Bentley R C and Nightingale K R 2004 Acoustic radiation force impulse imaging of the mechanical properties of arteries: *In vivo* and *ex vivo* results *Ultrasound Med. Biol.* **30** 1163–71

[10] Fahey B J, Nightingale K R, Nelson R C, Palmeri M L and Trahey G E 2005 Acoustic radiation force impulse imaging of the abdomen: demonstration of feasibility and utility *Ultrasound Med. Biol.* **31** 1185–98

[11] Tanter M, Touboul D, Gennisson J L, Bercoff J and Fink M 2009 High resolution quantitative imaging of cornea elasticity using supersonic shear imaging *IEEE Trans. Med. Imaging* **28** 1881–93

[12] Fatemi M and Greenleaf J F 1998 Ultrasound-stimulated vibro-acoustic spectrography *Science* **280** 82

[13] Chen S, Aquino W, Alizad A, Urban M W, Kinnick R, Greenleaf J F and Fatemi M 2010 Thermal safety of vibro-acoustography using a confocal transducer *Ultrasound Med. Biol.* **36** 343–9

[14] Fatemi M and Greenleaf J F 1999 Vibro-acoustography: an imaging modality based on ultrasound-stimulated acoustic emission *Proc. Natl. Acad. Sci. USA* **96** 6603

[15] Greenleaf J F, Fatemi M and Insana M 2003 Selected methods for imaging elastic properties of biological tissues *Annu. Rev. Biomed. Eng.* **5** 57–78

[16] Evans K D, Weiss B and Knopp M 2007 High-intensity focused ultrasound (HIFU) for specific therapeutic treatments: a literature review *J. Diagn. Med. Sonography* **23** 319

[17] Aubry J F, Pernot M, Marquet F, Tanter M and Fink M 2008 Transcostal HIFU: *ex vivo* adaptive focusing feasibility study *Phys. Med. Biol.* **53** 2937–51

[18] ter Haar G 1999 Therapeutic ultrasound *Eur. J. Ultrasound* **9** 3–9

[19] Dyson M 1995 Role of ultrasound in wound healing *Wound Healing: Alternatives in Management* ed J M McCulloch *et al* 2nd edn (Philadelphia, PA: FA Davis) pp 319–45

[20] Heckman J D, Ryaby J P, McCabe J, Frey J J and Kilcoyne R F 1994 Acceleration of tibial fracture-healing by non-invasive, low-intensity pulsed ultrasound *J. Bone Joint Surg.* **76** 26

[21] Carneiro A A O, Baffa O, Silva G T and Fatemi M 2009 Vibro-magnetometry: theoretical aspects and simulations *IEEE Trans. Ultrason. Ferroelectr. Freq. Control* **56** 1065

[22] Ilinskii Y A, Meegan G D, Zabolotskaya E A and Emelianov S Y 2005 Gas bubble and solid sphere motion in elastic media in response to acoustic radiation force *J. Acoust. Soc. Am.* **117** 2338

[23] Lenz J E 1990 A review of magnetic sensors *Proc. IEEE* **78** 973–89